Simulating Fringe Detection Techniques for an X-Ray Interferometer

Shashanth Sriramanathan

Supervisor: Phil Uttley

September 2024

Abstract

We build a simulator to test fringe detection techniques in a low photon count regime to be applied for X-Ray interferometers. Adopting methods from X-Ray spectral timing, we average periodograms to ensure good signal-to-noise ratios while minimizing effects of varying optical path differences. We find that, for a mono-wavelength scenario, the obtained signal-to-noise ratio agrees with predicted theoretical approximations.

1 Introduction

Current imaging capabilities has allowed imaging from radiowaves to ultraviolet to reach the diffraction limit through the use of interferometers and efficient optics. This is shown in fig 1, where the crosses mark the diffraction limit and the circles mark the resolution of the telescopes; the X-Ray telescopes have clearly not reached the theoretical limit. This is a problem, since the X-Ray sky makes up some of the most compact sources - from accretion processes onto compact objects to jets and shocks - and would greatly benefit from higher resolution imaging (these potential applications are detailed in Uttley, R. d. Hartog, et al. 2021). The development of an X-Ray Interferometer (XRI) would allow us to access these much higher resolutions.

The design of a proposed XRI is detailed in Uttley, R. d. Hartog, et al. 2020. This makes use of the Willingale design (Willingale 2004) which has the benefit of compacting the size of the interferometer by reducing the distance between the collector and the detector through the use of slatted mirrors, making it more viable to be launched aboard a satellite. A schematic of this is shown in fig 2.

Imaging for an XRI occurs through the fringe pattern produced by the interferometer, hence it is important to be able to resolve and detect the fringes. The

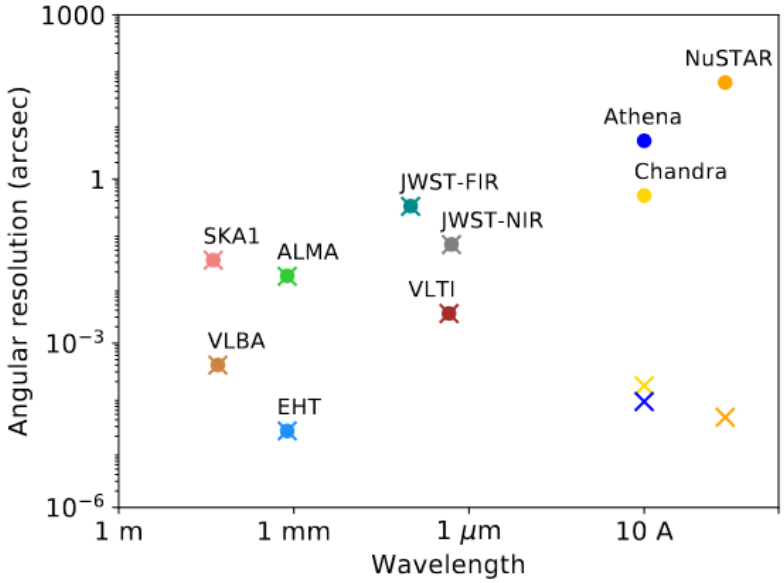

Figure 1: Comparing angular resolution of telescopes (circles) with diffraction limit (crosses). (Taken from Uttley, R. d. Hartog, et al. 2020, Figure 1)

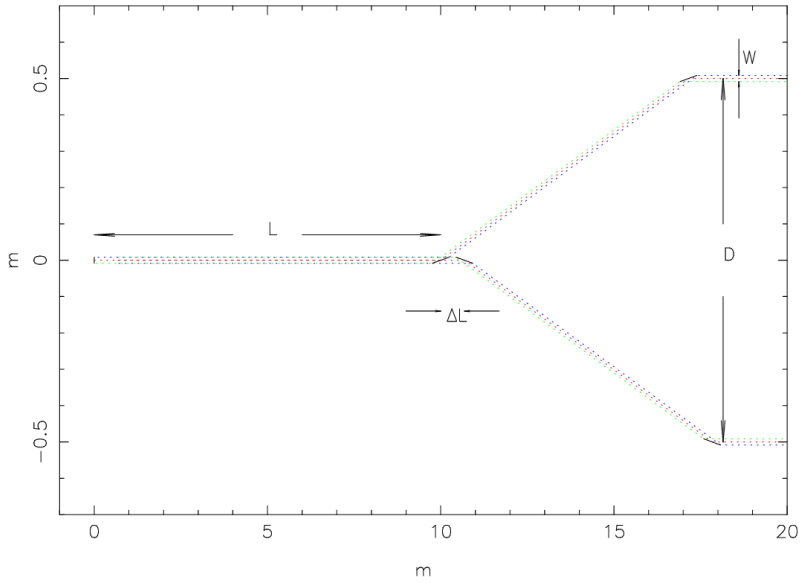

Figure 2: A schematic of the XRI setup with the important dimensions labeled. D is the baseline length and L is the separation between the region of maximum overlap and the second mirror. (Adapted from figure 4 of Willingale 2004).

fringe patterns are susceptible to very small changes in the optical path differences (due to the short X-Ray wavelengths), making the interferometer sensitive to vibrations and other disturbances that occur on short timescales and potentially smearing out the fringe pattern. This can be combated with exposure times that are short enough such that the optical path difference stays the same within a single exposure, but this would push us into a low photon-count regime. Hence, it is important to understand how fringe detection techniques work in this regime.

In order to study the effects of the low exposure times we simulate the fringe pattern and look at how the detectability of the fringes change while we vary the exposure time. This is especially useful as laboratory values for the stability timescales do not seem to be well known (Shipley, Cash, and Joy 2000).

The code is available at https://github.com/ShashanthS/XRI.

2 Methodology

We model the fringe pattern based on Willingale 2004 - this is briefly described in section 2.2. The simulator then works by sampling from the fringe pattern and stacking periodograms of each sample - this is explained in detail in section 2.2. Currently, the code only accounts for a single wavelength, future work is required to implement sampling from a range of wavelengths.

2.1 Fringe Pattern

In order to simulate readouts from single exposures, we need to sample the expected fringe pattern. This is done following the equations defined in Willingale 2004. This is briefly described here, for a more thorough explanation refer to the original paper.

The expected fringe pattern from the interferometer is modulated by Fresnel diffraction off the edges of the slits, resulting in the observed fringe pattern. This is described by the below equation

$$A_{obs} = A_{mod}(1 + exp(i\pi u_0 u)) \tag{1}$$

where A_{mod}[1] is the amplitude modulation and $(1 + exp(i\pi u_0 u))$ is the true fringe pattern. u and u_0 are dimensionless variables that are defined based on the coordinate of the central fringe, y'.

$$u = y'\sqrt{\frac{2}{\lambda L}} \tag{2}$$

y' is defined uniquely for the Fresnel diffraction component and the fringe pattern respectively. For the fringe pattern:

$$y'_{fringe} = \frac{-D\sin\theta}{2\sin(\theta_b/2)} \tag{3}$$

and for the Fresnel diffraction:

$$y'_{fresnel} = -L\theta \tag{4}$$

[1]This is obtained through Fresnel integrals, as described in Willingale 2004

where, in both cases, θ is the off axis angle. The main difference between the two is that the movement of the centre is dependant on L for the Fresnel pattern and on D for the fringe pattern. Three sets of sampled fringe patterns are shown in figure 3, where the off axis angles have been varied to show the pattern moving across the detector.

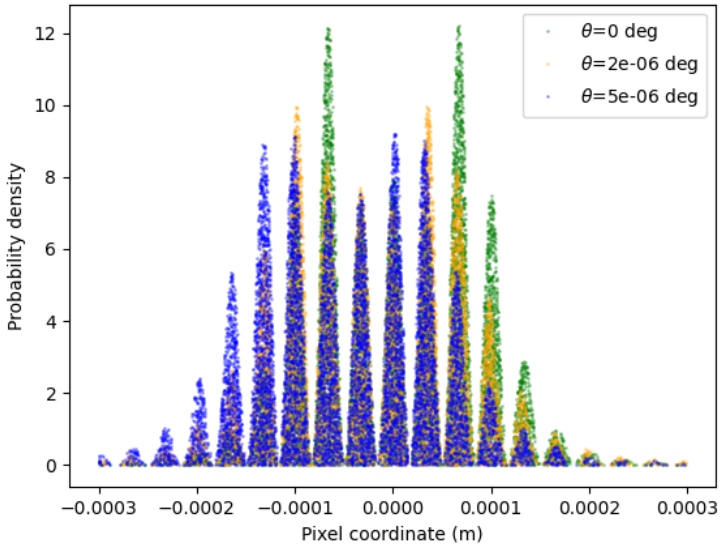

Figure 3: Fringe pattern for different off axis angles.

2.2 Sampling and Stacking

The number of photons per exposure is set by a poisson distribution, given the mean count rate. We assume that there is no changes in path length differences within a single exposure but allow for it between exposures. We create a periodogram for each exposure, then stack the periodograms for all the exposures. The result is then normalized. The process is highlighted below.

We define, according to Uttley n.d., the FT as:

$$a_k = \sum_j n_j \; exp(2\pi i \nu_k y_j) \tag{5}$$

and corresponding power as (in fractional rms normalization)

$$P_k = |a_k|^2 \tag{6}$$

We calculate the power P_k for each individual exposure and sum them. We normalize the summed periodograms using fractional rms normalization

$$P_{sum,rms} = \frac{2N}{n_{tot}^2}|a_k|^2 \tag{7}$$

where N is the number of experiments (i.e., the number of periodograms that are stacked).
Note that stacking periodograms allows us to remove the changes in path length differences between exposures. This is because the path length differences are phase terms in the Fourier transforms, which are removed when we take the modulus squared.

2.3 Detecting a Fringe

We want to figure out the point at which we can detect a significant fringe pattern. We do this by looking for the peak produced by the underlying sinusoidal function. The frequency of the underlying signal can be derived as below:

We know that the true fringe pattern is given by

$$A_{fringe} = 1 + exp(i\pi u u_0) \tag{8}$$

Hence, the intensity is obtained as

$$I = A_{fringe} A^*_{fringe} = (1 + exp(i\pi u u_0))(1 + exp(-i\pi u u_0)) \tag{9}$$

which simplifies to

$$I = 1 + 2cos(uu_0) = 1 + 2cos\left(\frac{2W}{\lambda L} y - y'_{fringe}\right) \tag{10}$$

From eqn 10, we can see that the frequency of the true fringe pattern is given by $\frac{2W}{\lambda L}$. If we now identify the noise level for the stacked periodogram, we can search for a significant peak at this known frequency.

2.3.1 Noise Level and Confidence Intervals

When using the fractional rms normalization, the noise level in the periodgram is given by

$$\langle P_{noise} \rangle = \frac{2}{\mu} \tag{11}$$

where μ is the average count rate. This can be approximated as (Uttley n.d.)

$$\langle P_{noise} \rangle = \frac{2}{\mu} \simeq \frac{2N_{bins}}{n_{tot}} \tag{12}$$

where N_{bins} is the number of fourier frequency bins and n_{tot} is the number of photons per exposure.

This noise is distributed in each bin of the periodogram according to a scaled χ^2_{2M} distribution:

$$P_{noise} \sim \frac{\langle P_{noise} \rangle}{2M} \chi^2_{2M} \tag{13}$$

where M is the number of stacked periodograms.

Note that this scaling gives us the expected mean noise level as

$$E[P_{noise}] = \frac{\langle P_{noise} \rangle}{2M} \times 2M = \langle P_{noise} \rangle \tag{14}$$

This also scales the variance as:

$$V[P_{noise}] = \left(\frac{\langle P_{noise} \rangle}{2M} \right)^2 \times 4M = \frac{\langle P_{noise} \rangle^2}{M} \tag{15}$$

Hence, the standard deviation is:

$$P_{noise,\,\sigma} = \frac{\langle P_{noise} \rangle}{\sqrt{M}} = err(P_{noise}) \tag{16}$$

If we have large enough samples, we can assume that the distribution becomes normal and use $P_{noise,\,\sigma}$ to define 3-σ confidence intervals.

3 Results

For the results highlighted below, unless mentioned otherwise, we use the following set of parameters:

- Baseline = 1 m
- $\theta = 0$ (*This is the off axis angle of the source in radians*)
- Beam width = 300 μm
- L = 10 m
- λ = 10 Å
- Readout rate = 24 Hz
- Ph_{ct} (photon count rate) = 20 s^{-1}

3.1 Verification of Noise Level

We ensured that our prediction for the noise level is accurate by calculating the average power in the high frequency region of the periodogram and comparing it with the theoretical value. We find good agreement in test runs hence we assume that the theoretical prediction are accurate in our experimental runs. The agreement can also be seen visually in fig 4.

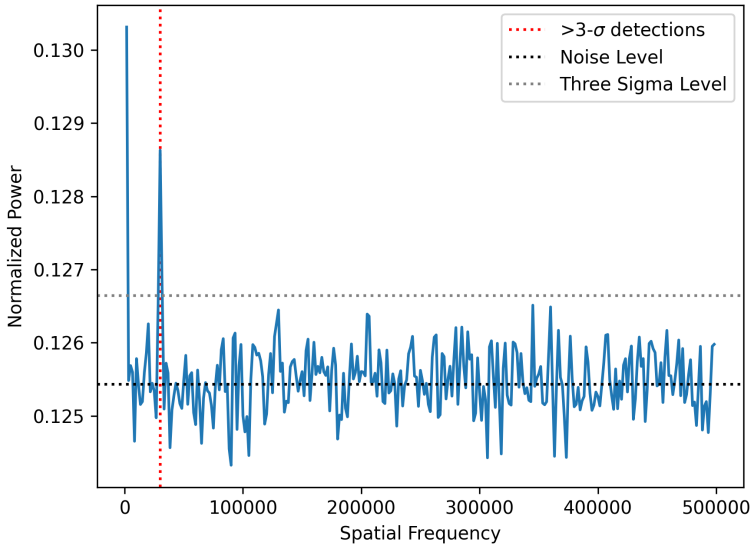

Figure 4: A sample result that shows that predictions of noise level agree with experimental values. The noise in the graph scatters around the dotted black line. The detected peak is marked as a red dashed line.

3.2 Detectability

To evaluate whether a specific set of parameters is likely to detect a fringe pattern, we conducted multiple experimental runs[2] using the same parameters and looked at the fraction of ru sn for which there was a significant peak. Additionally, a significance value, n_σ, was measured for each experimental run. This is defined as:

$$n_\sigma = \langle \frac{P_{fringe}}{err(P_{noise})} \rangle \tag{17}$$

where P_{fringe} is the Poisson noise subtracted power and the mean is taken over all the individual exposures - this is the snr. n_σ is then averaged over several runs of the experiment to get $\langle n_\sigma \rangle$, which is an average significance value. Table 1 shows the results for an assortment of exposure times (t_{exp}) and run times (T_{run}).

3.2.1 Exposure time scaling

We can test eqn 11 of Uttley n.d. (reproduced here in eqn 18) by varying the exposure time while keeping the run time constant.

$$\frac{\langle P_{fringe} \rangle}{err(\langle P_{noise} \rangle)} \simeq \frac{n_{tot}}{4} f_{samp}^{5/2} \sqrt{M} \tag{18}$$

For the exposure times that we consider, we are limited by the readout rate, making M constant. n_{tot} is linearly dependent on the exposure time: $n_{tot} = Ph_{ct} \times t_{exp}$ so we expect $\frac{\langle P_{fringe} \rangle}{err(\langle P_{noise} \rangle)}$ to scale linearly with n_{tot}.

[2] An experimental run is a single run of the simulator for a single set of parameters

Exp Time (s)	Run Time (s)	Success Rate	$\langle n_\sigma \rangle$
0.001	50000	24/25	5.65 ± 0.22
0.001	30000	22/25	4.40 ± 0.20
0.001	15000	12/25	3.25 ± 0.19
0.005	10000	24/25	12.19 ± 0.19
0.005	7000	25/25	9.97 ± 0.14
0.005	4000	25/25	7.39 ± 0.20
0.010	1000	50/50	7.67 ± 0.18
0.010	100	13/50	2.31 ± 0.15

Table 1: Results from experimental runs. Parameters as mentioned above.

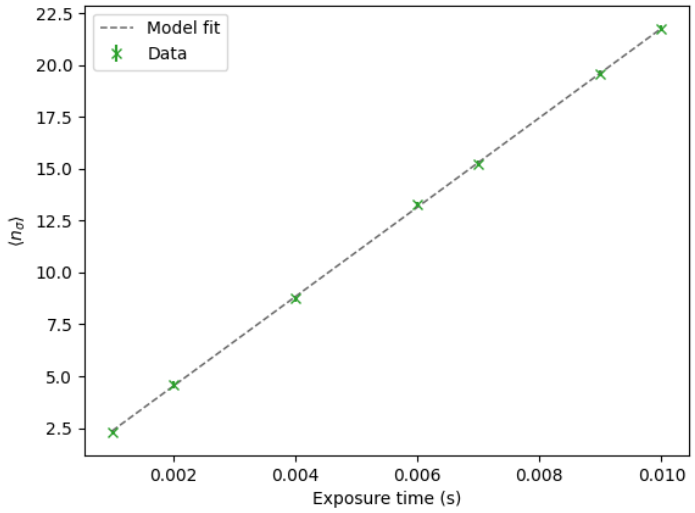

Figure 5: Relation between exposure time and n_σ. Note that the plot has error bars in n_σ but they are too small to be seen

As we can see from 5, our results produce the expected linear relation. To compare our results with what we expect from eqn 18, we fit a straight line ($y = mx + b$) to our result. This gives $m = 2158 \pm 11$ and $b = 0.20 \pm 0.08$. From 18, we get $m = 2190$ and $b = 0$ for the same parameters. These are in very good agreement, especially since we have assumed that $f_{samp} = 1$, which need not be exact for our simulation.

3.2.2 Run time scaling

Another question that could be important to ask is how $\langle n_\sigma \rangle$ varies with run time, for fixed exposure times. This is shown in figure 6.

From equation 18, we would expect $n_\sigma \propto \sqrt{T_{run}}$ since n_{tot} is fixed and $T_{run} \propto M$. This is what is seen in figure 6; the orange line is $y = \alpha\sqrt{T_{run}}$, where α is a scaling factor that has *not been fit*.

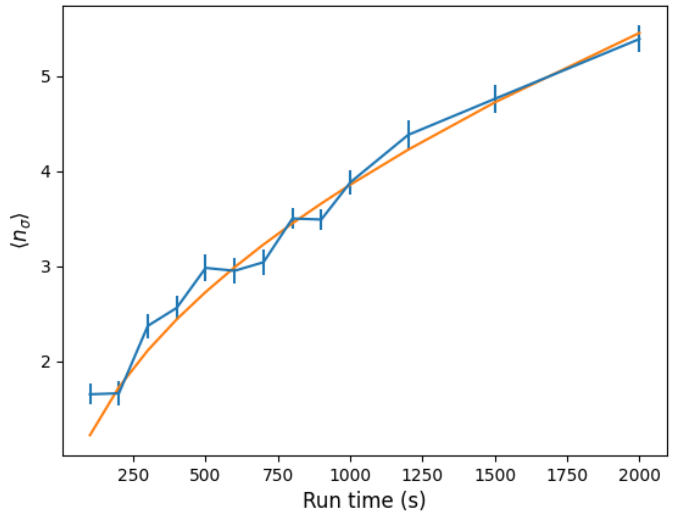

Figure 6: Relationship between n_σ and the run time. α is a scaling parameter that has been set to 8.2 to show that $n_\sigma \propto \sqrt{T_{run}}$

4 Discussion and Conclusion

In this report, we simulated a fringe detection technique, using periodograms, and studied the effects of low exposure times in the detectability of a fringe pattern. We found that changes in the optical path difference between different exposures had no effect on the detectability, as would be expected.

We get the expected scaling of $snr \propto n_{tot}$ and $snr \propto \sqrt{M}$ from equation 11 of Uttley n.d. We also find that the predicted snr values agree to our experimental results. *Hence we conclude that equation 11 from Uttley n.d. can be used while designing the experimental setups.*

The resolution of an XRI would be orders of magnitude higher than that of current X-Ray telescopes. For example, a 1 metre baseline would allow a resolution of 100 μas at 10 Å, while Chandra has a resolution of 0.5 arcseconds. Assuming that we know the location of an X-Ray source to around 0.1 arcsecond, if we want to image the source through an XRI, we would need to search a 1000*1000 grid of pixels to locate the source (assuming that the source is smaller than 1 pixel). A search algorithm which can efficiently search a given field for the presence of source, unique from the complete image reconstruction algorithm that would also be needed, is then crucial to have. The algorithm developed here - mainly, the idea of stacking periodograms - can be adapted to do this as its main goal is to look for fringes.

References

Shipley, Ann F., Webster C. Cash, and Marshall K. Joy (July 2000). "Grazing incidence optics for x-ray interferometry". In: *X-Ray Optics, Instruments, and Missions III*. Ed. by Joachim E. Truemper and Bernd Aschenbach. Vol. 4012. Society of Photo-Optical Instrumentation Engineers (SPIE) Conference Series, pp. 456–466. DOI: 10.1117/12.391584.

Willingale, Richard (Oct. 2004). "A practical system for x-ray interferometry". In: *SPIE Proceedings*. Ed. by Guenther Hasinger and Martin J. L. Turner. SPIE. DOI: 10.1117/12.552917. URL: http://dx.doi.org/10.1117/12.552917.

Uttley, Phil, Roland den Hartog, et al. (2020). "An x-ray interferometry concept for the ESA Voyage 2050 programme". In: *Space Telescopes and Instrumentation 2020: Ultraviolet to Gamma Ray*. Ed. by Jan-Willem A. den Herder, Shouleh Nikzad, and Kazuhiro Nakazawa. Vol. 11444. International Society for Optics and Photonics. SPIE, 114441E. DOI: 10.1117/12.2562523. URL: https://doi.org/10.1117/12.2562523.

Uttley, Phil, Roland den Hartog, et al. (June 2021). "The high energy Universe at ultra-high resolution: the power and promise of X-ray interferometry". In: *Experimental Astronomy* 51.3, pp. 1081–1107. DOI: 10.1007/s10686-021-09724-w. arXiv: 1908.03144 [astro-ph.HE].

Uttley, Phil (n.d.). "A Fourier approach to X-ray fringe finding". In: ().